Computerized Medical Imaging and Graphics 55 (2017) 106–112

Contents lists available at ScienceDirect

Computerized Medical Imaging and Graphics

journal homepage: www.elsevier.com/locate/compmedimag

Automatic detection of microaneurysms in retinal fundus images☆

Bo Wu, Weifang Zhu, Fei Shi, Shuxia Zhu, Xinjian Chen*

School of Electronic and Information Engineering, Soochow University, Suzhou, China

ARTICLE INFO

Article history:
Received 31 January 2016
Received in revised form 22 July 2016
Accepted 3 August 2016

Keywords:
Microaneurysms (MAs)
Diabetic retinopathy (DR)
Local features
Profile features
Classifier
Eye fundus images

ABSTRACT

Diabetic retinopathy (DR) is one of the leading causes of new cases of blindness. Early and accurate detection of microaneurysms (MAs) is important for diagnosis and grading of diabetic retinopathy. In this paper, a new method for the automatic detection of MAs in eye fundus images is proposed. The proposed method consists of four main steps: preprocessing, candidate extraction, feature extraction and classification. A total of 27 characteristic features which contain local features and profile features are extracted for KNN classifier to distinguish true MAs from spurious candidates. The proposed method has been evaluated on two public database: ROC and e-optha. The experimental result demonstrates the efficiency and effectiveness of the proposed method, and it has the potential to be used to diagnose DR clinically.

1. Introduction

Diabetic retinopathy (DR) is one of the main complications caused by diabetes. It is reported that DR has been the leading cause of new cases of blindness among adults between 20 and 60 years old (Walter et al., 2007). According to the World Health Organization (WHO), 347 million people were diagnosed with diabetes worldwidely (World Health Organization (WHO), 2016). It is also predicted that, by 2040, more than 640 million people may be living with diabetes (International Diabetes Federation, 2016).

In general, DR can be classified into two types: non-proliferative diabetic retinopathy (NPDR) and proliferative diabetic retinopathy (PDR) (Zhang et al., 2010), or six stages by the presence of different signs in retina. Most of the damage caused by DR can be reduced or prevented if it is diagnosed appropriately and regularly at the early stages.

However, it is a time-consuming work for an ophthalmologist to diagnose a diabetic patient manually, and it is also prone to error. Hence, automatic analysis of diabetic patients' retina is urgent needed for ophthalmologists to screen larger populations of patients.

In diabetic retinopathy, microaneurysms (MAs) are the important lesions. MAs appear as small and round shape dots near tiny blood vessels in fundus images. They are likely to be the only lesion, which present at the earliest stage of DR and remain in the development of the disease (Early Treatment Diabetic Retinopathy Study Research Group, 1991; Antal and Hajdu, 2012a). Therefore, detection of MAs is necessary and vital in a computer-aided screening system.

Fig. 1 shows a fundus image with several MAs. The diameter of MAs usually ranges from 10 μm to 100 μm (Pereira et al., 2014), which is considered less than the diameter of the major optic veins. Some objects of eye fundus images are similar to MAs in size and shape, which makes it diffcult to recognize MAs from them. One kind of them are small and round spots resulting from crossing of thin blood vessels. In fact, MAs should not lie on the vessels. In addition, vessel segments can also increase the difficulty of identifying MAs in fundus images, which appear as dark and small objects of various shapes. There are some studies recently for the diagnosis of MAs. In (Baudoin et al., 1984), Baudoin and Lay et al. proposed a computerized approach for detection of MAs in fluorescein angiograms, which was based on mathematical morphology method. The MAs were extracted from the FA by using different top-hat transformations. However, the FA were costly, invasive and not suitable for everyone, such as the pregnant woman (Walter et al., 2007). Besides, the method was very time-consuming. The conception of mathematical morphology was also applied in (Purwita et al., 2011). The MA candidates were extracted by removing vessels and small objects using canny edge detection and region filling algorithm. A post processing step was used to remove useless

☆ This work was supported in part by the National Basic Research Program of China (973 Program) under Grant 2014CB748600 and in part by the National Natural Science Foundation of China (NSFC) under Grant 81371629, 61401293, 61401294, 81401451, 81401472, and in part by Natural Science Foundation of the Jiangsu Province under Grant BK20140052.

* Corresponding author.
E-mail address: xjchen@suda.edu.cn (X. Chen).

http://dx.doi.org/10.1016/j.compmedimag.2016.08.001
0895-6111/

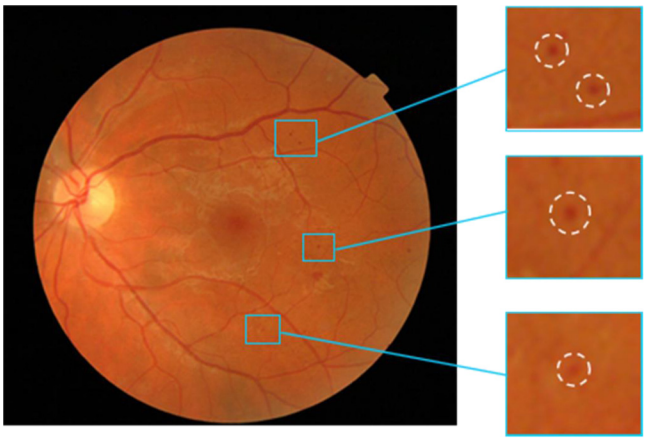

Fig. 1. An example of a fundus image with several MAs.

objects. Accurate detection of MAs was dependent on accurate detection of blood vessels and optic disc in this method. Spencer et al. (1992) proposed a method for detection of MAs using adaptive filters. Several features about intensity, size and shape of MA candidates were calculated. The disadvantages of the method were that it used FA images and was sensitive to the resolution of the FA images. Niemeijer et al. (Meindert et al., 2005) proposed a novel red lesion detection method based on a hybrid approach, which incorporated the previous works of Spencer et al. (1992) and Frame et al. (1998) with two new contributions. However, the total time of the method to process a single image was about 15 min, which was too long for screening systems. In Fleming et al. (2006), image contrast normalization was used to improve the ability to distinguish MAs from other dots in fundus image. The average execution time per image went from 53 s to 100 s. However, the sensitivity and specificity of the method were a little low for an efficient diagnostic tool. Template matching in the wavelet domain was proposed for detection of MAs in Gwénolé et al. (2008). By choosing appropriate sub-bands, the problems caused by illumination or high-frequency noise could be solved well without other image processing. In Antal and Hajdu (2012b), Antal proposed a novel ensemble-based system for MA detection and diabetic retinopathy grading. They improved MA detection by selecting the optimal combination of preprocessing methods and candidate extractors. An artificial neural network (ANN) (Gardner et al., 1996) was applied to recognize objects of diabetic fundus images, such as MAs, vessels and exudates. Convolution neural network (CNN) is a kind of artificial neural network. It is generally considered suitable for image recognition. The method was applied for detecting MAs by (Haloi, 2015) and achieved a sensitivity of 97% and a specificity of 95%. The disadvantage of these methods were the requirement for a large amount of training data and time-consuming. Lazar (Istvan and Andras, 2013) proposed a method for automatic detection of MAs through local rotating cross-section profile analysis. The local maximum pixels were selected as candidates. The cross-sectional scanning was applied to each candidate to produce 30 profiles. Then, peak detection was applied on each profile, and 7 properties of the peak was calculated. Several statistical measures of the resulting directional peak properties were as the set of features for a Bayesian classifier. In Seoud et al. (2015), a new set of shape features called Dynamic Shape Features was used for red lesion detection in fundus images. And, the Random Forest classifier was used for classification, which was a popular classifier widely used over the last few years (Jin et al., 2016; Jiang et al., 2016).

Motivated by Lazar's method (Istvan and Andras, 2013), in this paper, we propose a novel MA detection method with three important contributions. (1) A different candidate extraction method is used. In Istvan and Andras (2013), the candidates are extracted only based on peak detection, while in our method, the candidates are extracted based on not only the peak detection but also the region area and shape features. (2) A more robust preprocessing method is applied. The normalization of illumination and contrast limited adaptive histogram equalization (CLAHE) enhancement methods have been proposed to apply in the preprocessing step to enhance the input image for the following better candidate extraction and feature extraction. (3) In the feature extraction step, we have used much more features. A total of 27 features which contain not only profile features but also local features are used for classification.

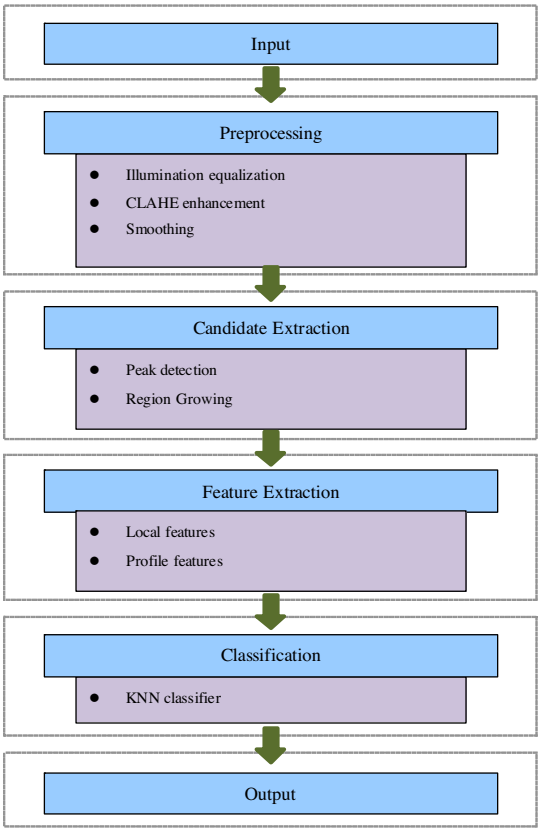

Fig. 2. Flowchart of the proposed method.

The rest of this paper is organized as follows. Section 2 describes the step of the proposed method in details. In section 3, the experimental results are present. Conclusion and discussion are presented in section 4.

2. Proposed method

2.1. Overview of the method

In the proposed method, the inverted green channel of fundus images is used as main input. The green channel provides the best MA-background contrast, while red channel is saturated. Blue channel is the darkest color channel and does not contain any information. Walter et al. (2007) explained why the green channel contained most of the image information. The binary region of interest (ROI) mask is also considered. The input images are required to have such spatial resolution that the diameter of their ROI is equal to 920 pixels. In fact, the proposed method can be applied on images of different spatial resolution by setting corresponding parameters.

The flowchart of the method presented in this paper is illustrated in Fig. 2. First, some necessary steps of preprocessing are

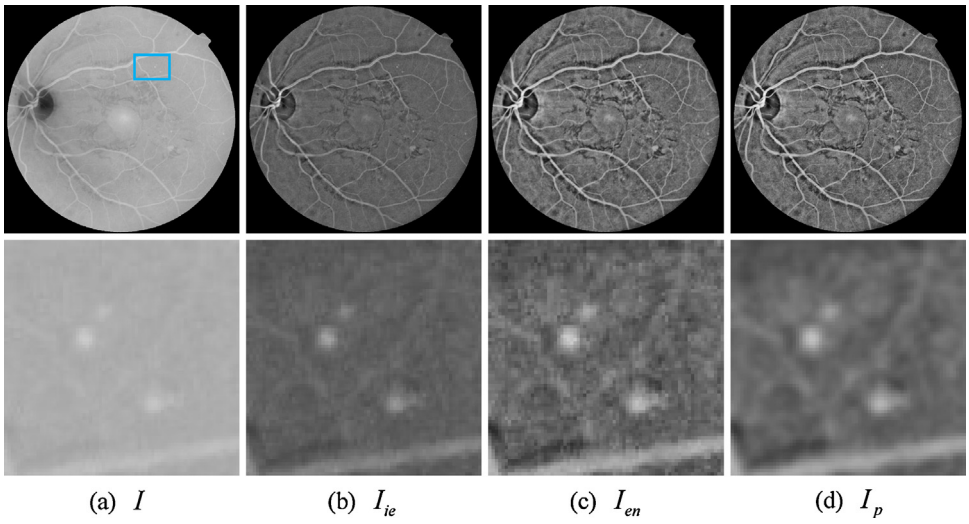

Fig. 3. The illustration of preprocessing steps. (a) Original inverted green channel image I; (b) illumination equalization image I_{ie}; (c) contrast limited adaptive histogram equalization enhancement image I_{en}; (d) the resulting image I_p after the step of smoothing. The lower row shows the details in blue rectangle after each step.

adopted to make MAs more visible. Second, the MA candidate regions are identified in the preprocessed image, based on the peak detection and region growing. Third, several features are extracted for classification. Finally, the KNN classifier is applied to distinguish true MAs from spurious candidates.

2.2. Image preprocessing

Retinal fundus images are often nonuniform illumination, poor contrast and noise images. MAs are hardly visible in regions of low brightness and poor contrast. In order to reduce these drawbacks and make a suitable image for MA candidate extraction and feature extraction, three preprocessing steps are applied as follow:

2.2.1. Illumination equalization

The illumination equalization method in Hoover and Goldbaum (2003) is used to correct shade as follows:

$$I_{ie} = I - I_{bg} + u \tag{1}$$

A mean filter of size 51×51 is applied to the original inverted green channel image I to generate a background image I_{bg}, which is used to estimate its illumination. Then, the I_{bg} is subtracted from the I to correct for shade variations. Lastly, the average intensity u of I is added to keep the same gray range as in the I.

2.2.2. Contrast limited adaptive histogram equalization (CLAHE)

In general, many MAs in the original inverted green channel fundus images do not have enough contrast with the surrounding background, which affects the next detection steps. In this paper, an enhancement method of contrast limited adaptive histogram equalization (CLAHE) (Zuiderveld, 1994) is applied to solve this problem. The enhancement technique is widely used in biomedical image processing and can make the interesting salient parts more visible effectively (Antal and Hajdu, 2012b).

2.2.3. Smoothing

Most of the available fundus images are stored in a lossy compressed form, which makes small structures such as MAs distorted. That is not conducive to extract extremely characteristic features of MAs. In addition, due to the small size of MAs, it is important to reduce the effect of noise. Thus, it is necessary to consider of a mountain of image smoothing before actual steps of detection. In our implementation, a Gaussian filter with a width of 7 and a variance of 1.0 is applied. The Fig. 3 shows an original inverted green channel fundus image and the resulting images processed by above steps.

2.3. Candidate extraction

The step of candidate extraction plays an important role in the whole detection. The main objective of this step is to reduce the number of objects which are not similar to MAs. However, any true MAs lost in this step can not be retrieved later. In this paper, the preliminary candidates are extracted by peak detection which is described in Istvan and Andras (2013). As MAs appear as bright structures in the preprocessed image, the MA region contains at least one regional maximum. Thus, the local maximum pixels can be considered as MA candidates. However, a large amount of noise will be extracted in this way. In order to overcome this limitation, peak detection is applied on each profile. In Istvan and Andras (2013), a set of line detectors of different orientations are applied to each local maximum pixel to examine the surrounding, whose central pixel is the local maximum pixel. And, a set of cross-section intensity profiles are obtained. Fig. 4 shows the intensity distribution of a profile. For each profile, peak detection is applied to decide whether a peak is present at the center of profile and seven properties of the peak are calculated. After peak detection, the peak can be represented by four descriptive values: IR_s, IR_e, DR_s and DR_e. In our implementation, 20 line detectors with 9° angular resolution are applied to generate 20 profiles. If any of the profiles which has no absolute difference between consecutive pixels larger than 5, the candidate is eliminated. The enhancement of CLAHE gains importance at this point. The method of CLAHE helps peak detection to eliminate most noise due to the fact that it is good at enhancing the contrast of MA while suppressing the noises.

However, the preliminary candidates can not represent the pathologies as found in the original retinal fundus image. Region growing is often used to grow MA candidate pixel back to the original pathology shape at candidate extraction step (Spencer et al., 1992; Meindert et al., 2005; Fleming et al., 2006). However, the growing threshold is hard to determine due to the variable intensity and size of MAs. In order to overcome these problems, in this paper, the dynamic transformation (Grimaud, 1992) which evaluates the regional maximum on a contrast criterion is applied.

If the preprocessed image is seen as a topographic surface, the dynamic of a local maximum is calculated as the difference in inten-

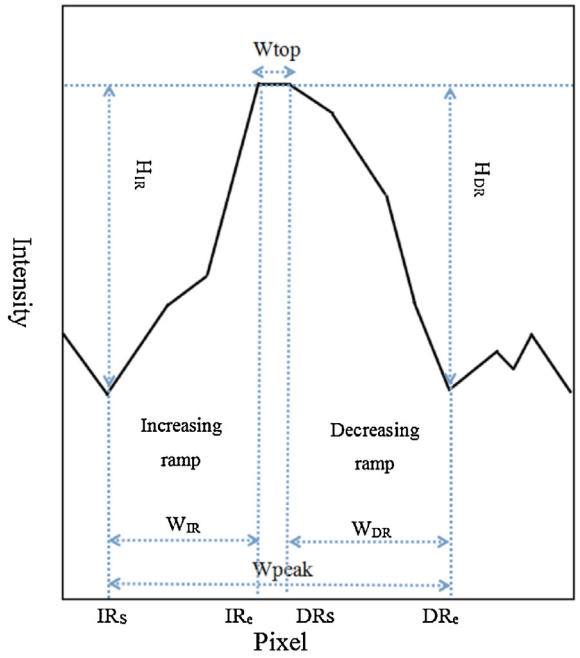

Fig. 4. The intensity distribution of a profile and the definitions of the peak.

sity between the given maximum and lowest pixel of the paths reaching a maximum of higher intensity. The original aspect of the dynamic transformation is that it does not consider the size and shape of the regional maximum. An adaptive threshold t based on the dynamic transformation can be calculated for region growing as follows:

$$t = i_{seed} - \beta * d_{seed} \tag{2}$$

where i_{seed} is the intensity of the starting position in the preprocessed image. In this paper, they are the preliminary candidate pixels. The d_{seed} is the dynamic value and $\beta \in (0, 1]$. Here, $\beta = 0.53$. Growing starts in the seed pixel and stops when there are no connected pixels higher than the threshold. Considering the MA's size is limited, every resultant connected component, which is lager than 140, will be discarded. In addition, elongated structures which are probably vessels can be discarded by area ratio r, which is calculated as follows:

$$r = \frac{S_{cand}}{S_{circle}} \tag{3}$$

where S_{cand} is the area of the candidate region and S_{circle} is the area of the candidate's circumcircle. The connected components will be also discarded, whose r is smaller than 0.5.

2.4. Feature extraction

The features proposed by Lazar (Istvan and Andras, 2013) derived from profile analysis. In this paper, we define these features as profile features. And three new profile features are added to improve the performance. But these profile features can not reflect overall characteristics of MAs well. Therefore, we also investigate a MA and its surroundings, and local features are proposed to add for the classification. Hence, in our classifier, besides profile features, local features are also used. The detail descriptions for features are given below.

2.4.1. Local features

2.4.1.1. Hessian matrix based features. The Hessian matrix is a square matrix of second-order partial derivatives of a scalar-valued function. It describes the local curvature of a function of many variables. Hessian matrix in 2D images is taken by second partial derivative from image's pixel and given as:

$$H(x, y) = \begin{bmatrix} D_{xx} & D_{xy} \\ D_{xy} & D_{yy} \end{bmatrix} \tag{4}$$

$$D_{xx} = G_{xx}(x, y; \sigma) * I(x, y) \tag{5}$$

$$D_{xy} = G_{xy}(x, y; \sigma) * I(x, y) \tag{6}$$

$$D_{yy} = G_{yy}(x, y; \sigma) * I(x, y) \tag{7}$$

where $I(x, y)$ is the preprocessed image, $*$ is convolution operator, and G_{xx}, G_{xy}, and G_{yy} are second-order Gaussian derivative along each direction.

Frangi et al. (2000) summarized the relations that must hold between the eigenvalues of the Hessian matrix for the detection of different structures. Let λ_1 and λ_2 be two eigenvalues ($|\lambda_1| \leq |\lambda_2|$). Because MAs appear as small, round and bright objects in preprocessed images, a MA-like probability map can be established by,

$$P_M(x, y; \sigma) = \begin{cases} 0 & \lambda_1 > 0 || \lambda_2 > 0 \\ \frac{2}{\pi} \arctan\left(\frac{|\lambda_2| + |\lambda_1|}{|\lambda_2| - |\lambda_1|}\right) & \lambda_1 \neq \lambda_2 \\ 1 & \lambda_1 = \lambda_2 < 0 \end{cases} \tag{8}$$

$$P_M(x, y) = \max_{\sigma_{\min} < \sigma < \sigma_{\max}} P_M(x, y; \sigma) \tag{9}$$

When P_M has a large value, the possibility of the pixel (x,y) belonging to a MA is high.

For each candidate regions, the following features are extracted:

- Mean of P_M, $|H|$.
- Max of P_M, $|H|$.
- Standard deviation of P_M, $|H|$.

Here, $|H| = \lambda_{1M} \times \lambda_{2M}$. λ_{1M} and λ_{2M} are the eigenvalues when P_M achieves the maximum. A total of 6 features are extracted.

2.4.1.2. Shape and intensity features. For extracting intensity and shape features, a sub-ROI is considered. The sub-ROI is nine times as large as the candidate region. The candidate region locates at the center of sub-ROI and the remaining region is as background. Besides, the shape of the sub-ROI is circular because MAs appear as round structure in the fundus images.

For each candidate region, the following shape and intensity features are extracted:

(1) The area $S = \sum_{j \in \Omega} 1$, where Ω is the set of pixels in the candidate region.
(2) The symmetry $R = \sqrt{\frac{1}{N_E} \sum_{j \in E} (d_j - \bar{d})^2}$, where d_j is the distance from an edge pixel to the brightest pixel (center pixel) of the candidate region. The $\bar{d}$ is the mean distance.
(3) The aspect ratio $P = \frac{l}{w}$, where l is the length of the largest and w is the second largest eigenvalue of the convariance matrix of the candidate region.
(4) The mean contrast of edge pixels. The contrast of a pixel can be calculated by $C = \frac{\sum_{j \in A} g_j}{N_A} - \frac{\sum_{j \in B} g_j}{N_B}$, where A is a set of pixels which belong to the 8-neiboring pixels of the calculated pixel and their intensity is greater or equal to calculated pixel. N_A is

the number of pixels belonging to *A*. *B*is the remaining pixels of 8-neiboring pixel.

(5) The standard deviation of edge pixels contrast $\sigma_C = \frac{\sum_{j\in Z}\sqrt{(C_j-\overline{C})^2}}{N_Z}$, where E is a set of edge pixels and N_E is the number of these pixels.

(6) The mean intensity of MA candidate region $M_{cand} = \frac{\sum_{j\in\Omega} g_j}{N}$.

(7) The standard deviation of MA candidate region intensity $\sigma_{cand} = \frac{\sum_{j\in\Omega}\sqrt{(g_j-M_{obj})^2}}{N}$.

(8) The mean intensity of background $M_{bg} = \frac{\sum_{j\in bg} g_j}{N_{bg}}$.

(9) The standard deviation of background intensity $\sigma_{bg} = \frac{\sum_{j\in E}\sqrt{(g_j-M_{bg})^2}}{N_{bg}}$.

(10) The difference between the mean intensity of MA candidate and its background $M_{diff} = M_{cand} - M_{bg}$.

(11) The difference between the maximal intensity of candidate region and a local contrast $D = g_{\max} - t$, where $t = M_{bg} - \beta\sqrt{\sigma_{bg}}$. It gives additional information about gray difference between MA candidate and its surroundings.

2.4.2. Profile features

(Istvan and Andras, 2013) Lazar (Istvan and Andras, 2013) used a total of seven different profile features during the classification. In this paper, three new useful profile features are added to improve performance. For better understanding, some necessary properties of the profile are also described here as follows:

1) The *peak width* is the difference between the start and end of the peak: $W_{peak} = DR_e - IR_s$.
2) The *increasing ramp height*: $H_{IR} = P[IR_e] - P[IR_s]$.
3) The *decreasing ramp height*: $H_{DR} = P[DR_s] - P[DR_e]$.
4) The *mean height* of the peak: $\overline{H_{peak}} = \sum_{IR_s}^{DR_e} P[i]/W_{peak}$.
5) The *start of increasing ramp height*: $H_{IR_s} = P[IR_s]$.
6) The *end of the decreasing ramp height*: $H_{DR_e} = P[DR_e]$.

The properties of 4–6 are new proposed in this paper to extract new features. After a whole peak detection finishes, every property set stores 20 values in this paper. Then, several statistical measures of the resulting directional peak properties are calculated. Three new sets are defined to store these values for better understanding. The *start of the increasing ramp* and the *end of the decreasing ramp height* values are stored in FHEIGHT set, likewise, the *mean height of the peak* values are stored in the MPHEIGHT. The PHEIGHT contains the *increasing and decreasing ramp height* values. Let σ_T denotes standard deviation of the values in set T. Thus, the first and second new features can be acquired by calculating $\sigma_{MPHEIGHT}$ and $\sigma_{FHEIGHT}$. These two features provide more information about how symmetric the candidate is. The third new feature is adopted to help eliminate the candidates locating in blood vessels. Let $\max_{height}$ and $\min_{height}$ donate the maximal value and minimal value of PHEIGHT set, respectively. The third feature is calculated as $R_{height} = (\max_{height} - \min_{height})/\min_{height}$. The candidates locating in the vessel have large R_{height} than the true MAs.

In summary, a total of 27 features (6 Hessian matrix + 11 shape and intensity + 10 profile) have been extracted for each candidate.

2.5. Classification

At the stage of feature extraction, each MA candidate is characterized by a vector in a 27-D feature set,

$$F = \{f_1, f_2, \ldots, f_{27}\} \tag{10}$$

However, the different feature f_i have different ranges and values, which is not good for some classifiers. Each of these features is normalized to zero mean and unit variance by applying,

$$\overline{f_i} = \frac{f_i - \mu_i}{\sigma_i} \tag{11}$$

where μ_i is the mean of the ith feature, and σ_i is its standard deviation. In order to select suitable classifier for the feature set, three supervised classifier are selected as the underlying classifiers: K-Nearest Neighbor (KNN), Naïve Bayes (NB) and Adaboost. We test the three classifier on the ROC database. And, the results show that the KNN (k = 14) and Adaboost have the similar performance and both outperform NB classifier. In this paper, the KNN (k = 14) classifier is selected for classification.

3. Results

3.1. Database

The proposed method has been tested on two public available database: e-ophtha and Retinopathy Online Challenge (ROC) database.

The e-ophtha is collected by E.Decencière and made of two sub databases called e-ophtha-MA (Microaneurysms) and e-ophtha-EX (Exudates). E-ophtha-MA comprises 148 fundus images with microaneurysms or small hemorrhages, which are manually annotated by ophthalmology experts. In this paper, 74 fundus images are used as training set and the remaining 74 fundus images as test set.

The ROC is a competition which aims to help patients with diabetes through improving computer aided detection. The ROC database is made up of 50 images for training and 50 images for testing. However, only the annotations of training set are public. Besides, Only 37 images of training set contain MAs, while the other 13 images do not contain any MA. Thus, in this paper, the 10-fold cross-validation is applied to evaluate the ability of classifiers when we use this database.

3.2. Assessment of classification performance

It is often not (Bunch et al., 1977) sufficient to simply detect the existence of MAs. Correct localization of the MAs is required for a true-positive detection. Therefore, in this paper, the free-response ROC (FROC) curve is used to evaluate the classification performance (Bunch et al., 1977). An FROC curve is a polt of operating points displaying the possible tradeoff between the sensitivity vs the average number of false positive detection per image. The sensitivity is calculated as follows:

$$sensitivity = \frac{TP}{TP + FN} \tag{12}$$

where TP denotes true positive and FN denotes false negative. The final score of a method is calculated as the average sensitivity at seven false positive rates (1/8, 1/4, 1/2, 1, 2, 4 and 8 false positives per image).

In this paper, the KNN classifier is selected for classification. Two other classifiers: Adaboost and NB are also evaluated on the ROC database to compare the performances. The corresponding FROC curves of classification results are plotted in Fig. 5. The evaluation

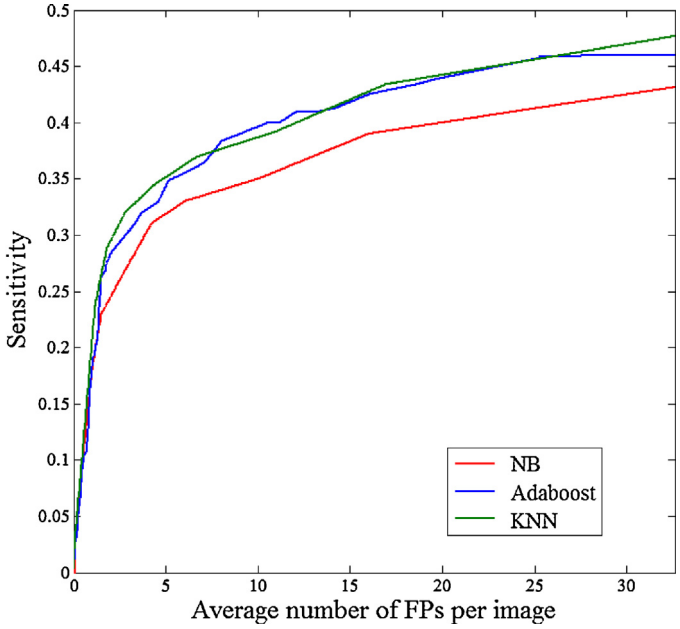

Fig. 5. The FROC curves of classification results by applying the KNN, NB and Adaboost classifiers to ROC database.

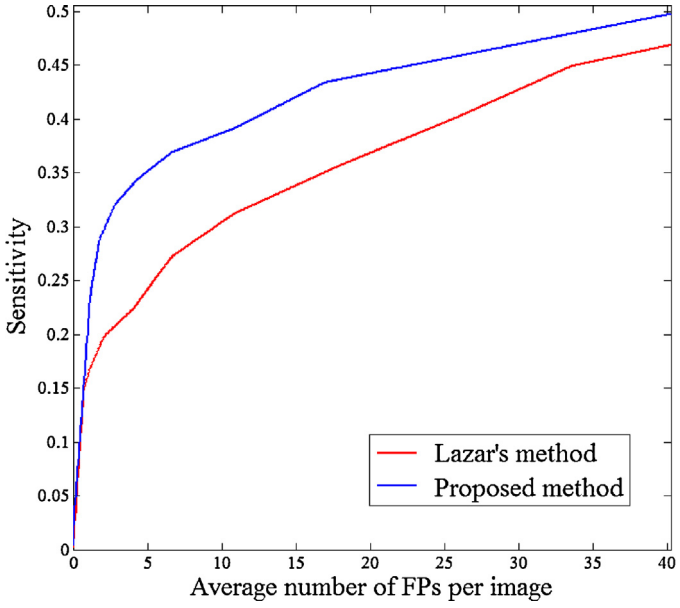

Fig. 6. The FROC curves of the proposed method and Lazar's method.

Table 1
Sensitivities At Predefined False Positive Per Image Rate For The Proposed Method And The Lazar's Method In The ROC Database.

	1/8	1/4	1/2	1	2	4	8
Lazar's method	0.037	0.055	0.103	0.162	0.196	0.223	0.285
Proposed method	0.037	0.056	0.103	0.206	0.295	0.339	0.376

results show that the KNN (k = 14) has the best performance. However, the Adaboost classifier has also very similiar performance, and they both outperform NB. The proposed method is also compared with Lazar's method (Istvan and Andras, 2013) on the ROC database. The classification of both methods use KNN classifier, because KNN classifier is also suitable for Lazar's method. Fig. 6 shows the FROC curve of the proposed method and Lazar's method. Table 1 shows the sensitivities at seven false positive rates (1/8, 1/4, 1/2, 1, 2, 4 and

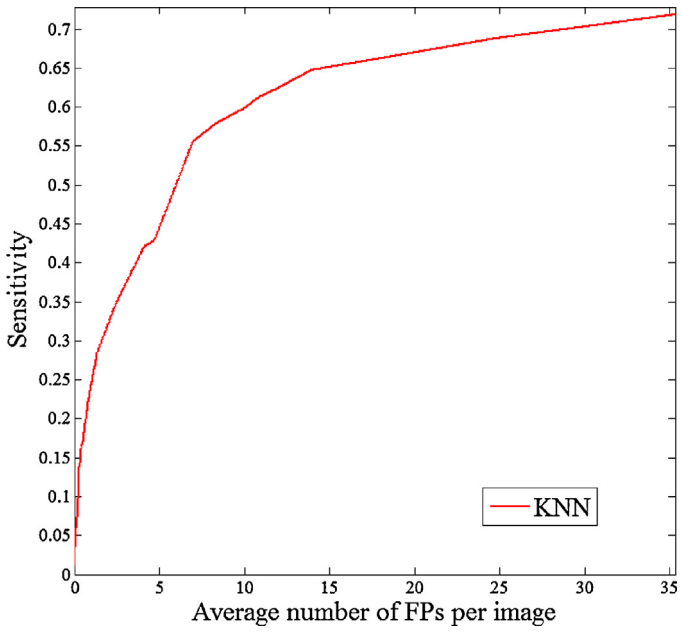

Fig. 7. The FROC curve of proposed method on the public database of e-ophtha-MA.

Table 2
Sensitivities At Predefined False Positive Per Image Rate For The Proposed Method In The E-ophtha-MA Database.

	1/8	1/4	1/2	1	2	4	8
Proposed method	0.063	0.117	0.172	0.245	0.323	0.417	0.573

8 false positives per image) for the proposed method and Lazar's method. Our method achieves an overall score of 0.202, which is better than 0.152 of Lazar's method.

The performance of the proposed method has also been evaluated on a public available database of e-ophtha-MA. The FROC curve is shown in Fig. 7 and corresponding seven sensitivities are shown in Table 2. The score of the proposed method achieves 0.273 on this database.

4. Discussion and conclusion

In this paper, we have proposed a method for automatic detection of MAs in fundus images. First, preprocessing steps are applied to enhance the input images for candidate extraction and feature extraction.A step of CLAHE enhancement is applied. The enhancement method of CLAHE has a good performance in making MA more visible while suppressing noises. The preliminary candidate pixels are extracted by applying peak detection on each profile. The region growing is adopted to grow preliminary candidate pixels back to original pathology shape, in which, the dynamic transformation is applied to obtain the optimal threshold. For feature extraction, 27 features are used which contain not only profile features but also local features. For classification, three classifiers of KNN, NB and Adaboost are compared and tested to find a suitable classifier for the feature set.

The proposed method has been evaluated on two public database: e-ophtha and ROC. The experimental results show that the KNN and Adaboost classifiers have similar classification performance and outperform Naïve Bayes classifier. Eventually, the KNN (k = 14) classifier is selected for classification in this paper. The proposed method is also compared with the method of Lazar. The result shows that our method has a better performance.

In summary, a fully automated and efficient methodology is proposed for detection of MAs. We believe this method has the potential to be used in diabetic retinopathy screen system.

References

Antal, B., Hajdu, A., 2012a. Improving microaneurysm detection using an optimally selected subset of candidate extractors and preprocessing methods. Pattern Recogn. 45 (1), 264–270.

Antal, B., Hajdu, A., 2012b. An ensemble-based system for microaneurysm detection and diabetic retinopathy grading. IEEE Trans. Biomed. Eng. 59 (6), 1720–1726.

Baudoin, C.E., Lay, B.J., Klein, J.C., 1984. Automatic detection of microaneurysms in diabetic fluorescein angiography. Revue D Épidémiologie Et De Santé Publique 32 (3–4), 254–261.

Bunch, P.C., Hamilton, J.F., Sanderson, G.K., et al., 1977. A free response approach to the measurement and characterization of radiographic observer performance. Proc. SPIE 4 (4).

Early Treatment Diabetic Retinopathy Study Research Group, 1991. Early photocoagulation for diabetic retinopathy. Ophthalmology 98, 766–785.

Fleming, A.D., Sam, P., Goatman, K.A., et al., 2006. Automated microaneurysm detection using local contrast normalization and local vessel detection. IEEE Trans. Med. Imaging 25 (9), 1223–1232.

Frame, A.J., Undrill, P.E., Cree, M.J., et al., 1998. A comparison of computer based classification methods applied to the detection of microaneurysms in ophthalmic fluorescein angiograms. Comput. Biol. Med. 28 (3), 225–238.

Frangi, Alejandro F., Niessen, Wiro J., Vincken, Koen L., Viergever, Max A., 2000. Multiscale vessel enhancement filtering. Lect. Notes Comput. Sci. 1496, 130–137.

Gardner, G.G., Keating, D., Williamson, T.H., et al., 1996. Automatic detection of diabetic retinopathy using an artificial neural network: a screening tool. Br. J. Ophthalmol. 80 (11), 940–944.

Grimaud, M., 1992. New measure of contrast: the dynamics. Image Algebra Morphol. Image Process. III, 292–305.

Gwénolé, Q., Mathieu, L., Pierre, Marie J., et al., 2008. Optimal wavelet transform for the detection of microaneurysms in retina photographs. IEEE Trans. Med. Imaging 27 (9), 1230–1241.

Haloi, M., 2015. Improved Microaneurysm Detection using Deep Neural Networks, Computer Science.

Hoover, A., Goldbaum, M., 2003. Locating the optic nerve in a retinal image using the fuzzy convergence of the blood vessels. IEEE Trans. Med. Imaging 22 (8), 951–958.

International Diabetes Federation, [Online] http://www.idf.org/wdd-index/.

Istvan, L., Andras, H., 2013. Retinal microaneurysm detection through local rotating cross-section profile analysis. IEEE Trans. Med. Imaging 32 (2), 400–407.

Jiang, X., Xiang, D., Zhang, B., et al., 2016. Automatic co-segmentation of lung tumor based on random forest in PET-CT images. SPIE Medical Imaging.

Jin, C., Shi, F., Xiang, D., et al., 2016. 3D fast automatic segmentation of kidney based on modified AAM and random forest. IEEE Trans. Med. Imaging 35 (6), 1395–1407.

Meindert, N., Bram, V.G., Joes, S., et al., 2005. Automatic detection of red lesions in digital color fundus photographs. IEEE Trans. Med. Imaging 24 (5), 584–592.

Pereira, C., Veiga, D., Mahdjoub, J., et al., 2014. Using a multi-agent system approach for microaneurysm detection in fundus images. Artif. Intell. Med. 60 (3), 179–188.

Purwita, A., Adityowibowo, K., Dameitry, A., et al., 2011. Automated microaneurysm detection using mathematical morphology. 2011 2nd International Conference on Instrumentation, Communications, Information Technology, and Biomedical Engineering (ICICI-BME). IEEE, 117–120.

Seoud, L., Hurtut, T., Chelbi, J., et al., 2015. Red lesion detection using dynamic shape features for diabetic retinopathy screening. IEEE Trans. Med. Imaging 35 (4), 1116–1126.

Spencer, T., Phillips, R.P., Sharp, P.F., et al., 1992. Automated detection and quantification of microaneurysms in fluorescein angiograms. Albrecht Von Graæes Archiv Für Ophthalmologie 230 (1), 36–41.

Walter, T., Massin, P., Erginay, A., et al., 2007. Automatic detection of microaneurysms in color fundus images. Med. Image Anal. 11 (6), 555–566.

World Health Organization (WHO), [Online] http://www.who.int/features/factfiles/diabetes/facts/zh/.

Zhang, B., Wu, X., You, J., et al., 2010. Detection of microaneurysms using multi-scale correlation coefficients. Pattern Recogn. 43 (6), 2237–2248.

Zuiderveld, K., 1994. Contrast limited adaptive histogram equalization. Graphics Gems, 474–485.